# IMPROVEMENT OF AERODYNAMIC PERFORMANCE OF A WINGED COMPOUND HELICOPTER DUE TO SINGLE-ROTOR LIFT-OFFSET

Hideaki Sugawara, sugawara.hideaki@jaxa.jp, Japan Aerospace Exploration Agency (Japan)
Yasutada Tanabe, tan@chofu.jaxa.jp, Japan Aerospace Exploration Agency (Japan)

**Abstract**
A system of single-rotor lift-offset combined with differential flaps on the fixed wing is investigated through numerical simulations. A simplified computational model consisting of a main rotor and a winged-body is utilized. The aerodynamic performance is evaluated in high-speed cruising flight where the advance ratio is 0.7. The effect of lift-offset on overall aerodynamic performance and the influence of aerodynamic interaction on the wing are investigated for the UH-60A rotor blade and the optimized rotor blade designed at JAXA. Numerical results show that the single-rotor lift-offset combined with the differential flaps significantly improves the overall aerodynamic performance for both rotors. The lift-offset dramatically enhances the rotor performance and minimizes the reduction of the aerodynamic performance of the winged-body due to the interaction with the rotor. Different interactional effects between the rotors with the wing are observed. It is observed that highly twisted blades significantly impact the wing under the advancing side due to the aerodynamic interactions.

## 1. INTRODUCTION

Compound helicopters are being researched and developed as one of the high-speed rotorcraft concepts. It is expected that the flight speed and the flight range can be dramatically increased than conventional helicopters. However, helicopters are known to have many aerodynamic interference issues as classified by Sheridan and Smith [1]. In their classification, the main rotor causes mutual interference with many airframe components. Winged compound helicopters are newly installed with a fixed-wing and multiple propellers used for antitorque devices and thrusters. Therefore, new aerodynamic interference issues arise for the fixed-wing and propellers, and new knowledge is required for the rotorcraft design.

Aerodynamic interactions between the rotor and the wing in forward flight have been reported by several researchers. Leishman and Bi investigated the aerodynamic interaction between the rotor and the lifting surface through wind tunnel test up to the advance ratio of 0.25 [2]. They indicated the effect of rotor wake on the wing aerodynamics and the influence of the blade passing over the wing on the wing pressure fluctuation. Brouwers et al. conducted a wind tunnel test of a compound helicopter to evaluate aerodynamic performance up to 0.45 for the rotor/wing aerodynamic interference [3]. Frey et al. investigated the mutual interference of the main rotor, wings, and lateral rotors at high-speed flight over the advance ratio of 0.5 for RACER configuration through numerical simulations [4]. The present authors also studied the rotor/wing aerodynamic interactions experimentally and numerically in high-speed flight [5-7]. These studies indicate several important points about the aerodynamic interaction phenomenon between the rotor and the wing: (1) Asymmetric aerodynamic load arises on the wing, (2) aerodynamic performance decreases significantly, and it depends on the rotor thrust (lift-share ratio of the rotor), (3) optimal lift-share ratio of the rotor is less than 10%. Since the aerodynamic performance is degraded by aerodynamic interaction, high-performance technology is required to realize an efficient winged compound helicopter.

Optimal design for rotorcraft components is an effective way to achieve high aerodynamic performance, but performance degradation due to the aerodynamic interaction remains. This paper focuses on lift-offset technology and attempts to improve the overall performance by increasing rotor performance.

The lift-offset technology has been applied to the coaxial rotors and it is reported that the rotor performance was significantly improved in forward flight [8-11]. For the single rotor, rolling moment of the rotor is required to create the lift-offset state. Thus, a system to cancel the rolling moment of the rotor is required to keep the rotorcraft attitude. There are several kinds of research on lift-offset for the single rotor. Reddinger and Gandhi studied the optimal trim states of a compound helicopter with an articulated rotor [12]. They investigated the effect on the aircraft lift-to-drag ratio by the single-rotor lift-offset state using the differential ailerons. The

Presented at 47th European Rotorcraft Forum, United Kingdom, 7-9th September, 2021

effective lift-to-drag ratios of the rotor and the vehicle was increased by the lift-offset. At the University of Maryland, a single rotor with a half-wing was investigated experimentally and numerically [13-15]. The half-wing was installed under the blade retreating side and created the required rolling moment. The single rotor cancels the rolling moment by the half-wing, resulting in a lift offset state. The results showed that the effective lift-to-drag ratio of the rotor and the wing remarkably increased due to the lift-offset.

This paper investigates the differential flap system to control the rolling moment of the wing and the single rotor lift-offset. The winged compound helicopter requires wing flaps to reduce the download from the rotor during hovering flight. The differential flap system utilizes these flaps. Even without the differential flaps, an asymmetric lift distribution on the wing is caused by the aerodynamic interaction with the rotor in high-speed flight. The lift of the wing under the blade advancing side is significantly decreased due to the induced velocity from the rotor. Under the retreating side, the wing aerodynamics is slightly influenced by the extensive reverse flow region. Thus, a rolling moment is caused on the winged-body by the aerodynamic interaction, and the rotor is already in a slight lift-offset state without flap deflections. Therefore, it can be expected that the lift-offset can be controlled by small flap deflections where the wing flap deflects upward under the blade advancing side and deflects downward under the blade retreating side. Additionally, with the small flap deflections, the increase in the drag of the wing can be minimized.

This paper aims to explore the effect of the lift-offset combined with the differential flaps on the aerodynamic performance of the winged compound helicopter. The aerodynamic performance is evaluated through numerical simulations, and a simplified compound helicopter consisting of a rotor and a winged-body is utilized. The effect of lift-offset on overall aerodynamic performance is investigated using two types of blades: an optimized rotor blade designed at JAXA [16] and a UH-60A rotor blade [17, 18] as the baseline. Differences in interference effects due to different blade shapes are also studied in this paper.

## 2. COMPUTATIONAL MODEL OF THE COMPOUND HELICOPTER

The compound helicopter model is based on JAXA's distinctive configuration [19, 20]. This rotorcraft is constructed with a single main rotor, a fixed-wing, two side propellers mounted at the fixed-wing tips as an antitorque device, and a pusher propeller at the aft of the fuselage as a thruster. The main rotor and the fixed-wing generate the lift. Also, the attitude of the rotorcraft is controlled by the main rotor. The tip-path plane is assumed to be perpendicular to the rotor shaft and parallel to the flight direction in high-speed cruising flight, where the rotor shaft angle is zero degrees.

### 2.1. Computational Model

Figure 1 shows the computational model. In order to focus on the aerodynamic performance of the rotor and the winged-body, the computational model is simplified and the propellers and the tail wings are omitted.

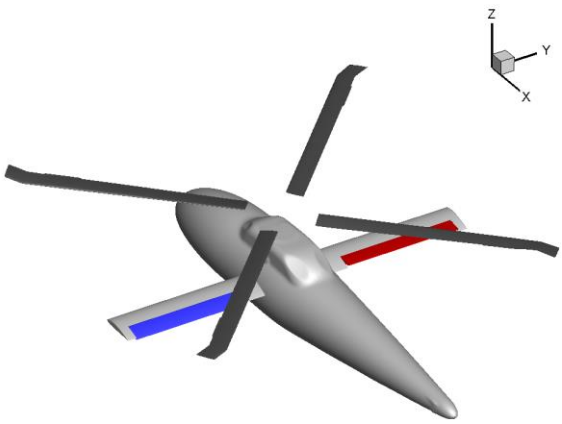


*Figure 1. Computational model for the assumed compound helicopter.*

The UH-60A blade and the optimized blade by JAXA as the main rotor blade are applied to the winged compound helicopter model in the present study. Both blade shapes are shown in Fig. 2.

(a) UH-60A rotor blade

(b) Optimized rotor blade (Opt-rotor)

*Figure 2. Blade geometry*

UH-60A blade [17, 18] has many published information. The rotor radius is 8.18 m. The blade has a large twist angle in a non-linear distribution. The equivalent linear twist is -16 degrees. The blade solidity is 0.082, and the equivalent blade chord length is 0.527. SC1095 and SC1094R8 airfoils are utilized. The optimized blade, called opt-blade in this paper, was designed for high advance ratio flight at

Presented at 47th European Rotorcraft Forum, United Kingdom, 7-9th September, 2021

JAXA [16]. The blade radius, solidity, and rotational speed are designed to be the same as UH-60A. The rotational speed is 258 RPM. The blade twist has a non-linear–distribution within $\pm 2$ degrees, which is much smaller than UH-60A. Elliptic airfoil is adopted in the blade inboard to aim for low drag in the extended reverse flow region. SC1095 airfoil is applied to the blade outboard. In high-speed cruising flight, the rotational speed of the main rotor is assumed to reduce to 75% RPM considering the compressibility effect.

The configuration of the winged-body is based on JAXA's distinctive configuration [20]. The specification of the main wing was determined, including the aerodynamic interaction effect, in the previous study [6]. The wingspan length is 11.452 m (70% of the rotor diameter). The aspect ratio is 10, the planform is a rectangle, and the airfoil is NACA4415. The vertical location of wing is assumed to be aligned with the fuselage center, and the distance from the rotor center 0.235 rotor radius. The incidence angle is selected at 5 degrees, where the lift-share ratio of the rotor is 0.23 obtained from the previous study without flaps [6]. The flaps in the main wing are mainly designed to aim for the reduction of the wing download in hover. The flap type is the plain flap, and the flaps are assumed to deflect up to 90 degrees, where the downward is positive. The span length of the flap on each side of the wing divided by the half wingspan, $b_h$, is $0.65 b_h$ (46% of the rotor radius, *R*). The chord length of the flap is $0.4 c_w$, where $c_w$ is the wing chord length.

### 2.2. Single-Rotor Lift-Offset System

Generation of rolling moment by the winged-body is required to achieve lift-offset with a single rotor. The lift-offset of a single rotor is defined as follows.

$$\text{Lift-offset} = \frac{M_x^{MR}}{L^{MR} R} = \frac{C_{Mx}^{MR}}{C_L^{MR}} \tag{1}$$

$$C_L^{MR} = \frac{L^{MR}}{\rho \pi R^2 (\Omega R)^2} \tag{2}$$

$$C_{Mx}^{MR} = \frac{M_x^{MR}}{\rho \pi R^2 (\Omega R)^2 R} \tag{3}$$

Where $M_x$ and $C_{Mx}$ is the rolling moment of the rotor and its coefficient, $L$ and $C_L$ is the lift of the rotor and its coefficient. The lift of the rotor is the same as the rotor thrust in this study because the shaft angle is zero. $\rho$ is the air density, $R$ is the main rotor radius, $\Omega$ is angular velocity. The differential flap system is proposed to be used to control the rolling moment of the winged-body in this study. Figure 3 illustrates the differential flap system. The differential flap generates an imbalance of lift on the left and right wings resulting in a rolling moment. The flap under the advancing side (Adv. side) deflects upward to reduce the lift, and the flap under the retreating side

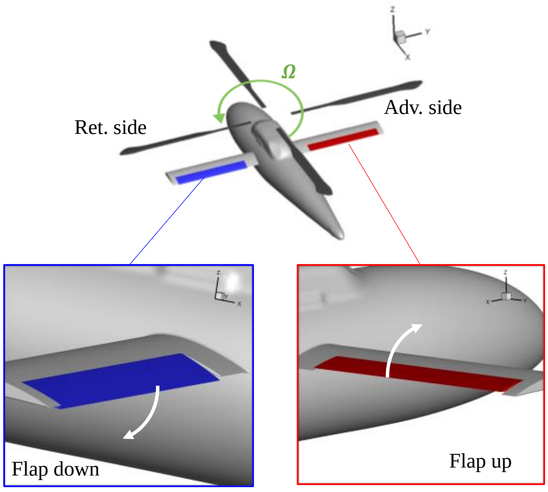


*Figure 3. Differential flap system.*

(Ret. side) deflects downward to increase the lift. The main rotor creates the opposite rolling moment against the winged-body and results in a lift-offset state. Even without the flaps, rolling moment of the winged-body occurs due to aerodynamic interaction between the rotor and the wing. Thus, this system is expected to obtain a large lift-offset by small flap deflections.

## 3. METHODOLOGY

### 3.1. Numerical Methods

A rotorcraft CFD solver, rFlow3D [21-24], developed at JAXA, is utilized to evaluate the aerodynamic performance of the compound helicopter. rFlow3D is one of the analysis tools within the multidisciplinary analysis toolchain for rotorcraft, including the trim analysis and the aeroelastic blade analysis.

rFlow3D is a structured grid solver based on a moving overlapped grid method. Additionally, an unstructured grid around a complex helicopter fuselage can also be included in the solution. The governing equations are three-dimensional compressible Navier-Stokes equations discretized with a finite-volume method. An all-speed numerical flux scheme, mSLAU (modified SLAU) [21], calculates the inviscid flux. The viscous flux is computed using a second-order central difference scheme. Time integration methods are provided by an explicit four-stage Runge-Kutta method [25] for the background grids and LU-SGS [26] implicit unsteady method extended by dual time-stepping method for the body-fitted grids. A fourth-order compact MUSCL TVD (FCMT) interpolation method [27] is applied to achieve higher-order spatial accuracy. The Menter *k*-*ω* SST 2003 turbulence model [28] is adopted in this study. Tri-linear interpolation method is used for interpolations between the overlapped grids.

The trim analysis is performed every half rotor revolution by loosely coupling with CFD simulations. The blade controls are changed by the trim analysis based on the averaged rotor aerodynamic forces and moments. The trim adjustment is based on the partial derivatives of the rotor thrust and moments to the rotor controls using a delta form [5, 23]. The forces and moments of the rotor generated by the CFD have averaged values for one rotor revolution. The partial derivatives are numerically obtained based on the blade element theory (BET). The sectional aerodynamic forces in BET are computed using the two-dimensional airfoil aerodynamics table. The blade control angles are updated with a relaxation factor to improve computational stability and convergence.

### 3.2. Simulation Setup

Simulations are performed based on the assumed cruising flight conditions, 420 km/h (227 kt), corresponding to an advance ratio of 0.7 of the rotor. The target lift is defined as the gross weight of the rotorcraft of 97,861 N based on the maximum takeoff weight of the UH-60A helicopter [29]. The main rotor adjusts the overall lift, rolling moment, and pitching moment by the collective pitch angle and the cyclic pitch angles. The rotor rotational speed is reduced to 75% RPM from the hover RPM at high-speed flight. Table 1 summarized the assumed cruising flight condition.

Table 1 Assumed flight condition

| | |
|---|---|
| Flight condition | Cruise (420 km/h) |
| Attitude angle | 0 degrees |
| Rotor tip Mach number | 0.4875 |
| Rotor advance ratio | 0.703 |
| Gross weight | 97,860 N ( $C_W = 1{,}38 \times 10^{-2}$ , nondimensionalized by 75% RPM.) |
| Target rolling/pitching moments | 0.0 Nm |
| Differential flap angles | 0, $\pm 2°$, $\pm 4°$, $\pm 5°$ |

The blade is assumed to be a very stiff blade with minimal elastic deformation. Thus, the blade is simulated as a rigid blade in this study. Also, the flapping and the lead-lag motion are also assumed zero.

Moving overlapped grids are utilized to simulate the high-speed cruising flight. Figure 4 shows the grid system used in the present study. The outer and inner background grid captures the complex vorticity flowfield around the assumed compound helicopter. The background grids are Cartesian grids. The outer background grid has a stretched grid distribution, and the inner background grid has a uniform grid distribution. The spatial grid resolution in the inner background grid is set to 15% of the blade tip chord length of UH-60A, which is 0.561 m. The outer background grid has a uniform grid distribution within the region overlapped with the inner background grid. The grid size in this region is two times the size of the inner background grid. The blade and winged-body girds are the body-fitted grid. The first grid spacing from the wall corresponds to a y-plus of less than 1.0.

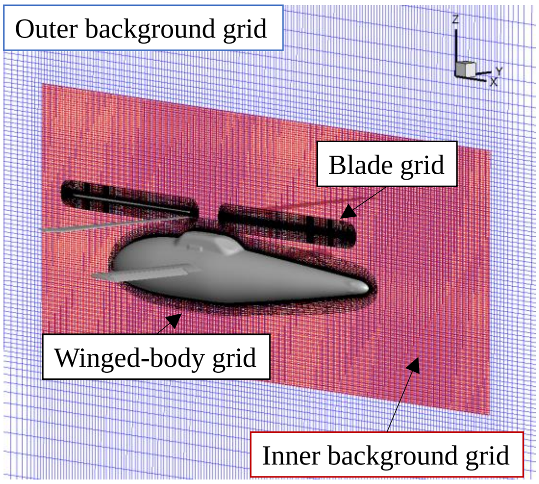


*Figure 4. Moving overlapped grid system used in the present study.*

Partial overlapping grids are applied to simulate the differential flap deflections. Figure 5 shows an example of the partial overlapping grids. The flap grid is overlapped with the winged-body grid and the inner background grid. Chimera grid methodology is applied to determine the calculation grid. Octree search and an Alternating Digital Tree (ADT) [30] are adopted to accelerate the hole-cut procedure. The interpolation grid is defined as the boundary condition and exchanges the physical quantities between the other grids. Also, the blank grid, a non-calculated grid, is determined when it exists inside another body.

Figure 6 shows an example of convergence history of the blade control angles, which are the collective pitch angle $\theta_0$, the lateral cyclic pitch angle $\theta_{1c}$, and the longitudinal cyclic pitch angle $\theta_{1s}$, by the trim adjustment. All of the blade control angles are converged after 10 rotor revolutions. Figure 7 shows the convergence history of the lift. The rotor and the winged-body generate the rotorcraft lift, and it can be seen that the total lift converges to the target lift. All cases converged to the target lift within an error of 0.2%. Figure 8 shows the convergence history for the

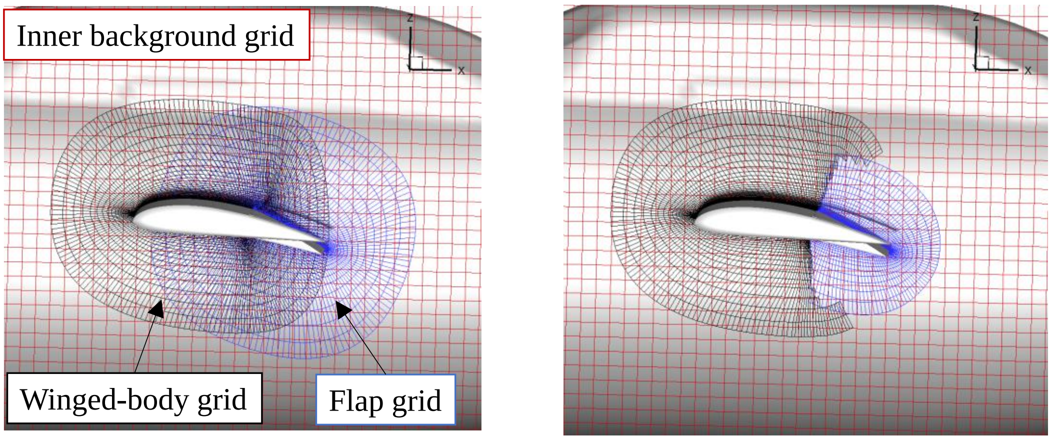


(a) Before the hole-cut procedure. (b) After the hole-cut procedure.

*Figure 5. Overlapping grid of the winged-body with the flap grid.*

rolling and pitching moments. The total rolling and pitching moments of the rotor and the winged-body are trimmed to zero moments. These histories show the case of UH-60A rotor with 0degrees flap. The interesting point is that the rolling moment on the winged-body occurs due to the aerodynamic interaction between the rotor and the wing. The rotor generates the counter-rolling moment to achieve the zero moments and is already in the lift-offset state. The details of the results are described in the next section.

## 4. RESULTS AND DISCUSSION

The aerodynamic performance of the assumed compound helicopter is evaluated through the overall effective lift-to-drag ratio. The overall effective drag has computed the sum of the effective drag of the rotor, $C_{DE}^{MR}$, and the drag of the winged-body, $C_D^{WB}$.

$$system\ C_{DE} = C_{DE}^{MR} + C_D^{WB} \tag{4}$$

$$C_{DE}^{MR} = \frac{C_P^{MR}}{\mu} + C_D^{MR} \tag{5}$$

$$C_P^{MR} = \frac{P^{MR}}{\rho \pi R^2 (\Omega R)^3} \tag{6}$$

$$C_D^{MR} = \frac{D^{MR}}{\rho \pi R^2 (\Omega R)^2} \tag{7}$$

$$C_D^{WB} = \frac{D^{WB}}{\rho \pi R^2 (\Omega R)^2} \tag{8}$$

Also, $\mu$ indicates the advance ratio of the rotor.

$$\mu = \frac{V_\infty \cos i}{\Omega R} \tag{9}$$

$i$ is the incidence angle of the rotor, where this value is zero degrees in the present study.

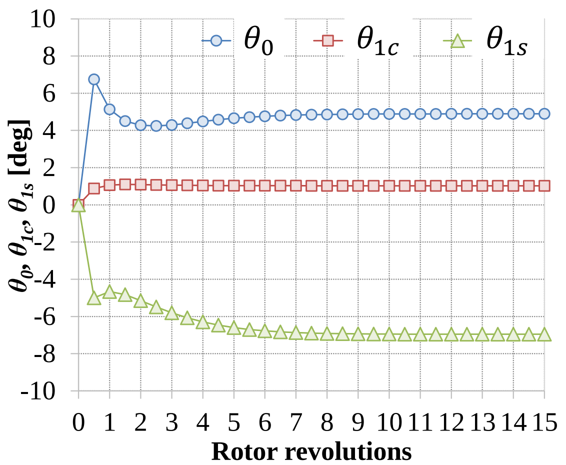


*Figure 6. Convergence history of the blade control angles in case of UH-60A rotor with 0degrees flap deflection.*

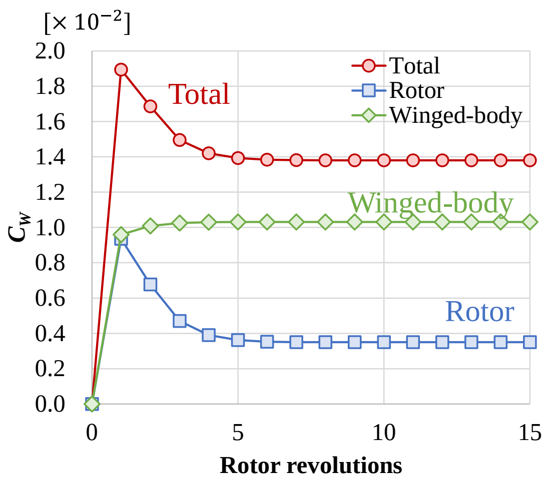


*Figure 7. Convergence history of the lift in case of UH-60A rotor with 0degrees flap deflection.*

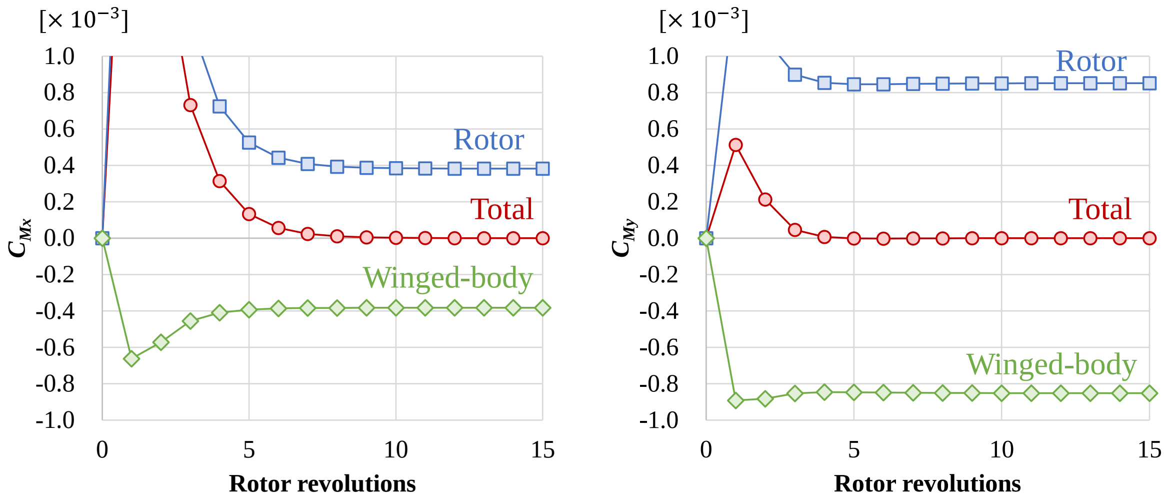


(a) Rolling moment

(b) Pitching moment

*Figure 8. Convergence history of the rolling and pitching moments in case of UH-60A rotor with 0degrees flap deflection.*

The rotorcraft lift is a total of the rotor and the winged -body.

$$system\ C_L = C_L^{MR} + C_L^{WB} \tag{10}$$

$$C_L^{WB} = \frac{L^{WB}}{\rho\pi R^2(\Omega R)^2} \tag{11}$$

### 4.1. Effect of Lift-Offset due to Differential Flaps

The lift-offset of the single rotor is generated by the asymmetric lift distribution on the wing due to the aerodynamic interaction and the differential flap deflections in this study. Figure 9 shows the sectional lift distribution on the wing by the differential flap deflections in the case of the UH-60A rotor. The sectional lift and drag are expressed below.

$$c_l = \frac{l}{1/2\,\rho U_\infty^2 c_w} \tag{12}$$

$$c_d = \frac{d}{1/2\,\rho U_\infty^2 c_w} \tag{13}$$

It can be seen that the asymmetric lift distribution on the wing is obtained as aimed. The lift on the wing for the opt-rotor shows similar distributions. The effect of aerodynamic interactions with the two rotors will be discussed the next section.

Figure 10 shows the obtained lift-offset values for the single rotor by the differential flap deflections. The maximum lift-offset values for both rotors are obtained at the differential flap deflections of 5 degrees. The values of lift-offset are 0.4 for the UH-60A rotor and 0.36 for the opt-rotor, respectively. It is an interesting point that the lift-offset arises due to the aerodynamic interaction even with zero flap deflection, 0.10 for the UH-60A and 0.04 for the opt-rotor, respectively. The difference in the lift-offset

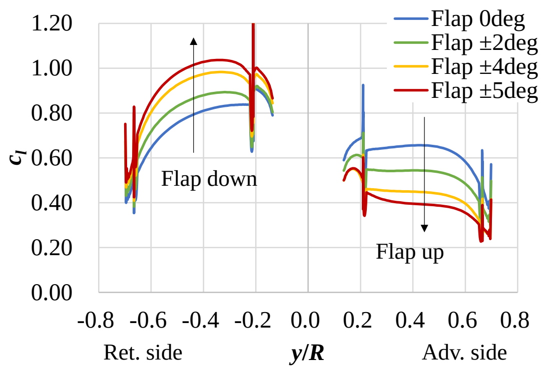


*Figure 9. Sectional lift distributions due to the differential flap deflections in the case of the UH-60A rotor.*

values is caused by the effect of aerodynamic interaction on the wing with different type of rotors.

Figure 11 shows the lift-share ratio of the rotor against the differential flap deflections for both rotors. The lift-share ratios of the UH-60A rotor have large values relative to the opt-rotor due to the different interactional effects of the rotor on the wing. The lift-share ratios are 0.24 to 0.27 for the UH-60A rotor and 0.22 to 0.25 for the opt-rotor.

The overall effective lift-to-drag ratios for the two rotors are shown in Fig. 12. The overall effective lift-to-drag ratio improves with increasing of the lift-offset. The lift-to-drag ratio increases by 10% compared with zero flap deflections, and the opt-rotor is higher than the UH-60A rotor. The opt-rotor was designed

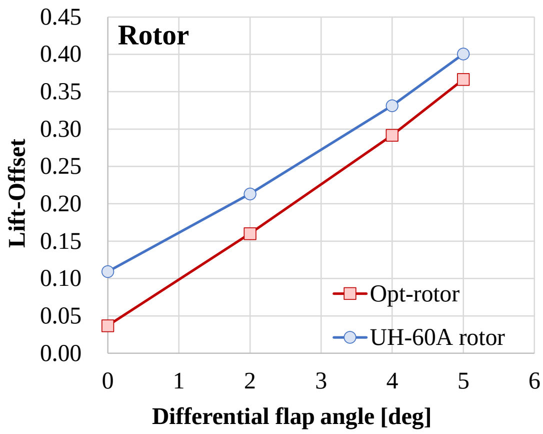


*Figure 10. Obtained lift-offset for the single rotor by the differential flap deflections.*

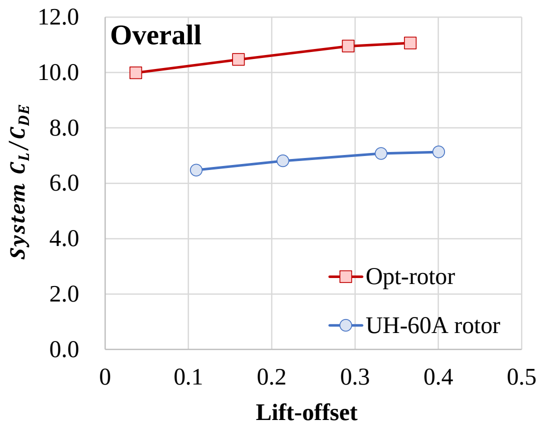


*Figure 12. System effective lift-to-drag ratio compared between the UH-60A rotor and the opt-rotor.*

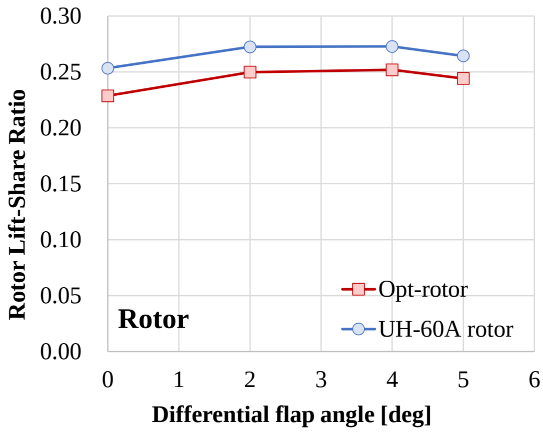


*Figure 11. Lift-share ratios for both rotors.*

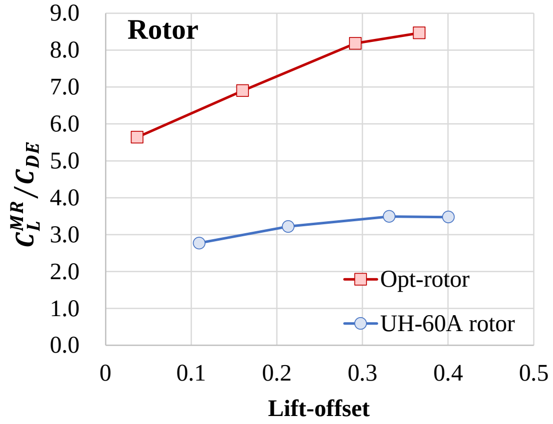


*Figure 13. Effective lift-to-drag ratio of the rotor.*

for high-speed flight and was obtained with high aerodynamic performance. Therefore, it is clear that the combination of improved rotor performance through optimization and lift-offset technology by the differential flap system can further enhance the overall aerodynamic performance.

The aerodynamic performance of each rotor and the winged-body are examined to understand their contributions to the overall lift-to-drag ratio. Figure 13 shows the effective lift-to-drag ratios for both rotors. The opt-rotor performance provides higher aerodynamic performance, approximately two times of the UH-60A rotor. The lift-to-drag ratio of the opt-rotor is enhanced by approximately 50% at the lift-offset of 0.37 compared with zero flap deflections. On the other hand, the lift-to-drag ratio of the UH-60A improves 25% at the lift-offset of 0.40 compared with zero flap deflections. Note that the rotor thrusts of both rotors are different, and the effect of lift-offset may vary with the lift-share ratio of the rotor. This point will be studied as future works.

The increasing lift-to-drag ratio means the reduction of the effective drag of the rotor. The effective drag of the rotor is defined by the rotor power and the drag as shown in eq. (3). Thus, the rotor performance improvement sensitivity can be understood from the trend of the change in rotor power and drag.

Figure 14 shows the rotor power against the lift-offset. The power coefficient of the opt-rotor is significantly reduced by 28% at the lift-offset of 0.37 compared to zero flap deflections. For the UH-60A rotor, only a small change in power coefficient is observed.

Figure 15 shows the drag coefficient against the lift-offset. The drag of the rotor decreases when the lift-offset increases for both rotors. In the UH-60A rotor, the drag is remarkably reduced by 27% at the lift-offset of 0.37 compared with zero flap deflection. These results indicate that the sensitivity for the performance improvement depends on the blade shape.

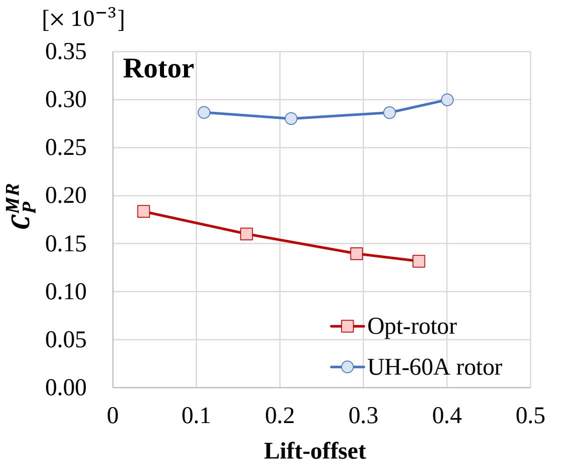


*Figure 14. Rotor power coefficients against the lift-offset.*

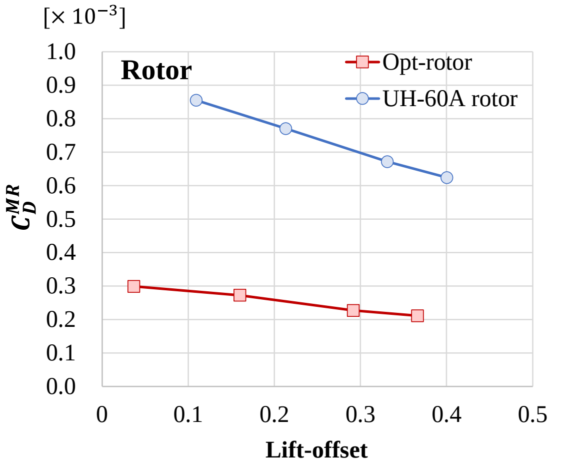


*Figure 15. Rotor power coefficients against the lift-offset.*

The blade controls are examined to understand the performance improvement mechanism. Figure 16 shows the blade control angles, the collective pitch angle, and the lateral and longitudinal cyclic pitch angles. The decreasing trends in the blade control angles are observed with increasing of lift-offset. This tendency is the same as the performance improvement by lift-offset for the coaxial rotors [11, 31].

The lift-offset reduces the collective pitch angle to generate the lift in the advancing side, where the dynamic pressure is higher than the retreating side. In addition, the cyclic pitch angles are decreased because the required lift for moment balance is reduced on the blade retreating side. Reducing the blade control angles due to the lift-offset is expected to enhance the control limit of the rotor during high-speed flight.

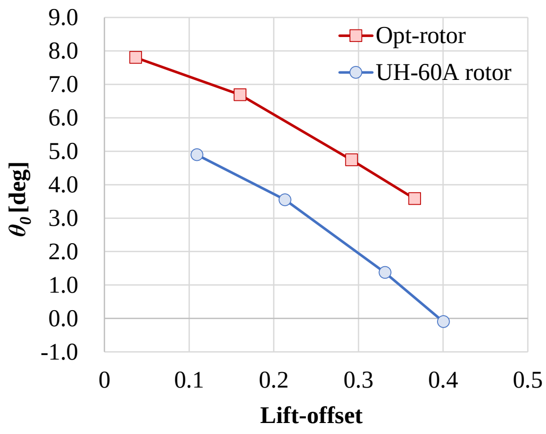


(a) Collective pitch angle, $\theta_0$

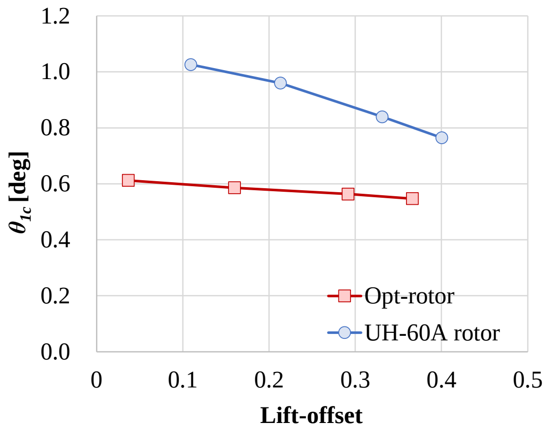


(b) Lateral cyclic pitch angle, $\theta_{1c}$

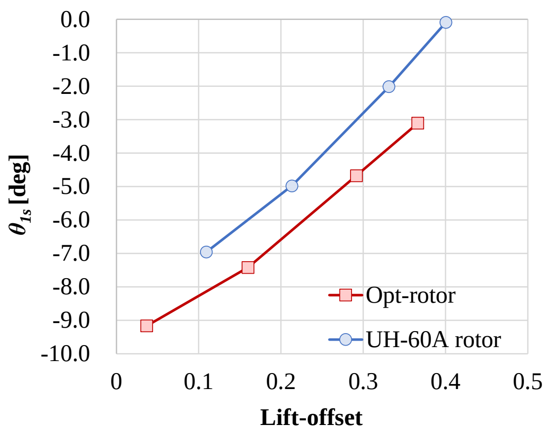


(c) Longitudinal cyclic pitch angle, $\theta_{1s}$

*Figure 16. Blade control angles against the lift-offset*

For the UH-60A rotor with highly twisted blade, the profile drag is larger due to the larger projected area relative to the freestream velocity. As the pitch angle of the blade decreases, the profile drag reduces, which in turn decreases the drag of the rotor. The change in the blade pitch angle is a small contribution to the rotor power because the pitch angle at the blade tip is slight due to the large twist angle.

For the opt-rotor with a small twisted blade, the large blade pitch angle increases the sectional chord force at the tip, which contributes ~~sensitively~~ dominantly to the change in rotor power. The reduction of the collective pitch angle also contributes to the decrease in the projected area of the blade relative to the freestream velocity, resulting in the reduction of the drag of the rotor. Therefore, the lift-offset reduces both power and drag of the rotor for the small twisted blade.

Figure 17 shows the sectional normal force, $C_n M^2$, distributions at each azimuth angle for both rotors in the conditions of differential flap angles of zero and 5 degrees. At zero flap deflections, both rotors mainly generate the lift in front of the rotor. The opt-rotor appears to produce lift significantly in the front. The location of the main lift forces changes to the blade advancing side due to the lift-offset. An extensive area of negative lift is identified in the opt-rotor at zero flap deflections, and this region disappears by the lift-offset when the flap differential deflection angle is 5 degrees.

Also, the normal force of the UH-60A rotor at zero flap deflections is mainly produced on the advancing side, and the change in distribution due to the lift-offset is less noticeable than the opt-rotor. Therefore,

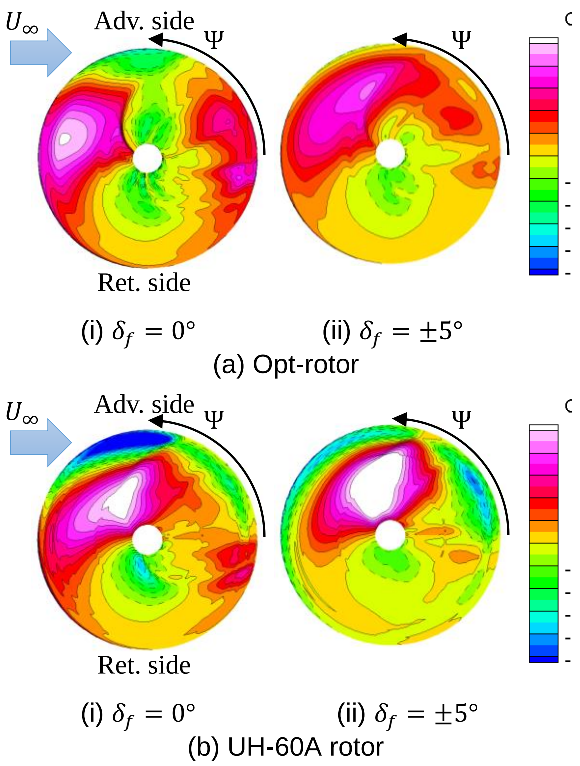


*Figure 17. Sectional normal force distributions.*

an important point to improve rotor performance is to change the lift generated in the front to the advancing side where the dynamic pressure is high by the lift-offset. The effect of the lift-share ratios on the performance improvement due to the lift-offset of both rotors should be further investigated.

Figure 18 shows the lift-to-drag ratio of the winged-body. The lift-to-drag ratio decreases with increasing of the lift-offset because of the large flap deflections. The maximum reduction in the lift-to-drag ratio is 3% for the UH-60A and 5% for the opt-rotor. Please note that this difference is caused by the difference of the rotor design and will be discussed in the next section. The performance degradation caused by the differential flap deflections was relatively small, as originally intended.

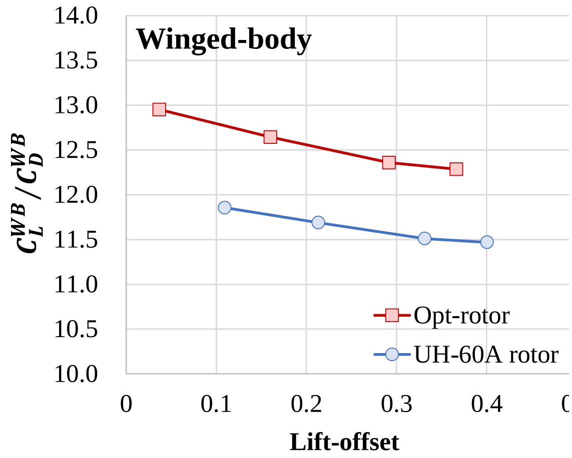


*Figure 18. Lift-to-drag ratio of the winged body against the differential flaps.*

Figure 19 shows the lift and drag coefficients nondimensionalized by the rotor parameters, as shown in Eq. (6) and (10). The lift of the winged-body decreases due to the flap deflection. The drag of the winged-body also increases due to the flap deflections. The flap should be designed to provide sufficient lift-offset before the drag increases significantly.

## 4.2. Effect of Aerodynamic Interaction

In the previous section, the effect of aerodynamic interference varies depending on the blade shape. The influence of the aerodynamic interference on the wing due to the rotor shape is discussed below.

Figure 20 shows the sectional lift and drag coefficient on the wing with zero flap deflections. Both sectional forces on the wing are asymmetrically distributed. Previous studies have indicated that the sectional lift on the wing decreases, and the sectional drag on the

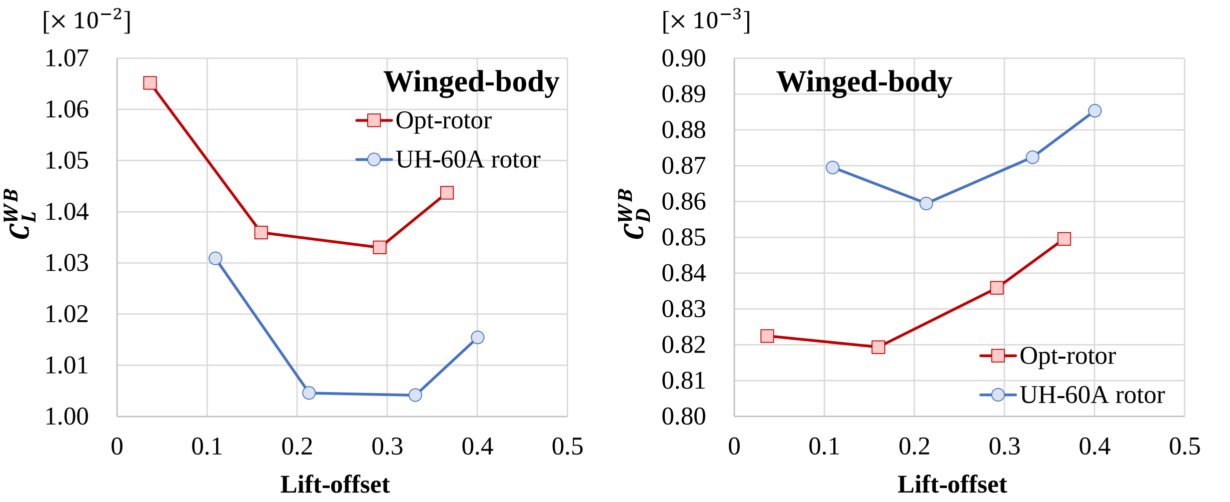


(a) Lift coefficients (b) Drag coefficients

*Figure 19. Lift and drag coefficient of the winged-body against the differential flaps.*

wing increases under the blade advancing side (Adv. side) due to the induced velocity from the rotor [5, 6]. Under the retreating side (Ret. side), the sectional forces have little effect due to the small induced velocity by the extended reverse flow region.

Comparing the sectional lift coefficient on the wing between both rotors under the blade advancing side, the lift coefficient of the UH-60A is lower than the opt-rotor. Similarly, the sectional drag under the advancing side of the UH-60A is higher than the opt-rotor. It indicates that the UH-60A rotor causes stronger aerodynamic interaction to reduce aerodynamic performance of the wing.

Additionally, under the retreating side, it can be observed that the sectional aerodynamic performance of the wing with the opt-rotor reduces partially than with the UH-60A. It implies that the induced velocity distribution from the rotor around the wing is different between the rotors.

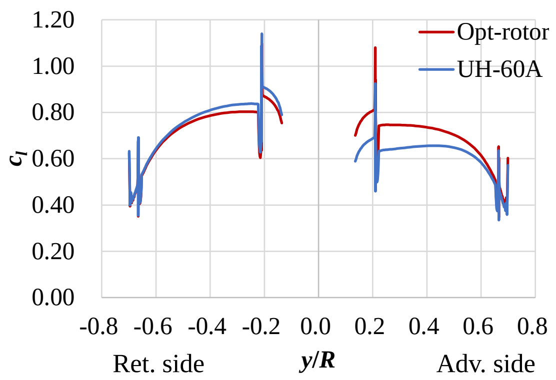


(a) sectional lift coefficient

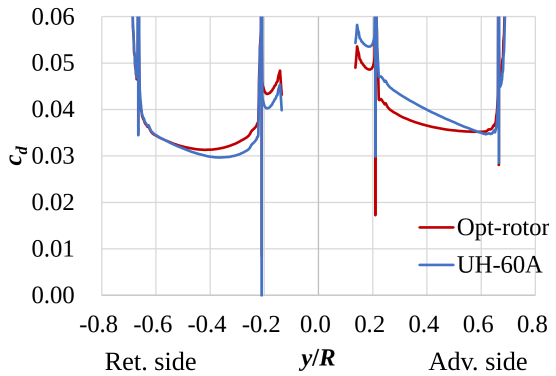


(b) sectional drag coefficient

*Figure 20. Comparison sectional forces on the wing with zero flap deflections between the opt-rotor and the UH-60A rotor.*

The induced velocity distribution around the wing is related to the sectional normal force distribution of the rotor [6]. In comparison to the sectional normal force, $C_n M^2$, distribution between both rotors in the case of zero flap deflections as shown in Fig. 17, a large sectional normal force on the advancing side is partially observed for the UH-60A. The blade on the inboard has a large blade angle due to the large twist. Thus, large sectional lift is produced on the inboard region at the advancing side because of high dynamic pressure. The UH-60A rotor causes larger induced velocity than the opt-rotor, and the larger induced velocity increases the inflow angle to the wing and reduces the aerodynamic performance. Therefore, the interference effect with the UH-60A rotor is more significant than the opt-rotor. A highly twisted blade can significantly impact the wing under the advancing side due to the aerodynamic interactions.

Although a large sectional normal force of the opt-rotor is distributed toward the advancing side, the retreating side also generates a certain amount of sectional normal force. Thus, the opt-rotor noticeably affects the aerodynamics of the wing at the retreating side under these conditions. Since the induced velocity distribution is based on the sectional normal force, the effect of the aerodynamic interaction on the wing is different for both rotors, as shown in Fig. 20.

## 5. CONCLUSIONS

A system of single-rotor lift-offset combined with the differential flaps is investigated through numerical simulations. A simplified computational model consisting of the main rotor and the winged-body is utilized. The aerodynamic performance is evaluated in high-speed cruising flights where the advance ratio is 0.7. The effect of lift-offset and the influence of aerodynamic interference on the wing are examined for the UH-60A rotor blade and the optimized rotor blade designed at JAXA. The following conclusions are obtained.

1. The lift-offset combined with the differential flaps significantly improves the overall aerodynamic performance for both rotors. Specifically, the overall effective lift-to-drag ratios increase by 10% at differential flap angle of 5 degrees compared with zero flap deflections for both rotors.
2. The lift-offset dramatically improves the rotor performances for both rotors. In this study, the UH-60A rotor increases by 25%, and the opt-rotor increases by 50%. The reduction of the aerodynamic performance of winged-body is minimized due to the differential flap deflections.
3. The lift-offset reduces the required blade control angles to satisfy the trim conditions by effectively utilizing the advancing side with high dynamic pressure. It is expected to extend the control limit of the rotor during high-speed flight.
4. Different interactional effects between both rotors and the wing are observed. Highly twisted blades may significantly impact the wing under the advancing side due to the aerodynamic interactions.

## REFERENCES


[1] Sheridan, P. F., and Smith, R. P., "Interactional Aerodynamics—A new Challenge to Helicopter Technology," Journal of the American Helicopter Society, Vol. 25, No. 1, Jan. 1980, pp. 3-21.

[2] Leishman, J. G., and Bi, N., "Experimental Investigation of Rotor/Lifting Surface Interactions," Journal of Aircraft, Vol. 31, No. 4, July–Aug. 1994, pp. 846–854.

[3] Brouwers, E., Fillmax, M., and Deresz, R., "Advanced AH-64 Compound Wind Tunnel Testing Overview," Proceedings of Vertical Flight Society 75th Annual Forum, Philadelphia, Pennsylvania, May 2019.

[4] Frey, F., Thiemeire, J., Öhrle, C., Keßler, M., and Krämer, E., "Aerodynamic Interactions on Airbus Helicopters' Compound Helicopter RACER in Cruise Flight," Proceedings of Vertical Flight Society 75th Annual Forum, Philadelphia, Pennsylvania, May 2019.

[5] Sugawara, H. and Tanabe, Y., "Numerical Investigation of Rotor/Wing Aerodynamic Interactions at High Advance Ratios," Journal of Aircraft, Vol. 56, No. 6, Nov.–Dec. 2019, pp. 2285-2298.

[6] Sugawara, H., Tanabe, Y., and Kameda, M., "Effect of Lift-Share Ratio on Aerodynamic Performance of Winged Compound Helicopter," Journal of Aircraft, Mar. 2021.

[7] Tanabe, Y., Sugawara, H., Kobiki, N., Kobayashi, W., Hayashi, H. and, Sato, R., "Experimental and Numerical Investigation of Interaction Between Rotor and Wing at High Advance Ratio," Proceedings of Vertical Flight Society 76th Annual Forum, Virtual, Oct. 5–8, 2020.

[8] Bagai, A., "Aerodynamic Design of the X2 Technology DemonstratorTM Main Rotor Blade," American Helicopter Society 64th Annual Forum, Montreal, Canada, April 29-May 2008.

[9] Walsh, D., Weiner, S., Arifian, K., Lawrence, T., Wilson, M., Millott, T., and Blackwell, R., "High Airspeed Testing of the Sikorsky X2 TechnologyTM Demonstrator," Proceedings of American Helicopter Society 67th Annual Forum, Virginia Beach, VA, May 2011.

[10] Johnson, W., "Influence of Lift Offset on Rotorcraft Performance," NASA/TP-2009-215404, Nov. 2009.

[11] Ho, J. C., and Yeo, H., "Analytical study of an isolated coaxial rotor system with lift offset," Aerospace Science and Technology, 100, 105818, 2020.

[12] Reddinger, J. and Gandhi, F., "Physics-Based Trim Optimization of an Articulated Slowed-Rotor Compound Helicoter in High-Speed Flight," Journal of Aircraft, Vol. 52, No. 6, Nov.–Dec. 2015, pp. 1756-1766.

[13] Wang, X., Maurya, S. and Chopra, I., "Slowed Hingeless Rotor Wind Tunnel Tests and Validation at High Advance Ratios," Journal of Aircraft, Vol. 58, No. 1, Jan.–Feb. 2021, pp. 153-166.

[14] Maurya, S., Wang, X., and, Chopra, I., "Wind Tunnel Test on a Slowed Mach-Scaled Hingeless Rotor with Lift Compounding," Proceedings of Vertical Flight Society 76th Annual Forum, Virtual, Oct. 5–8, 2020.

[15] Maurya, S., Chopra, I., and, Datta, A., “In Search of Extreme Limits if a Compound Helicopter in High Speed Flight,” Proceedings of Vertical Flight Society 77th Annual Forum, Virtual, May 10–14, 2021.
[16] Sugiura, M, Tanabe, Y., Sugawara, H., and Takekawa, K., “Optimal Design of Rotor Blade for a Winged Compound Helicopter at High Advance Ratio,” Proceedings of Vertical Flight Society 76th Annual Forum, Virtual, Oct. 5–8, 2020.
[17] Bousman, W. G., “Aerodynamic Characteristics of SC1095 and SC1094R8 Airfoils,” NASA T2003-212265, AFDD/TR-04-003, Dec. 2003.
[18] Davis, S. J., “Predesign Study for a Modern 4-Blade Rotor for the RSRA,” NASA CR 166155, March 1981.
[19] Tanabe, Y., Aoyama, T., Kobiki, N., Sugiura, M., Miyasita, R., Sunada, S., Kawachi, K., and Nagao, M., “A Conceptual Study of High Speed Rotorcraft,” Proceedings of 40th European Rotorcraft Forum, Royal Aeronautical Soc. Paper 33-B, Southampton, UK, Sept. 2014.
[20] Tanabe, Y., Sugiura, M., Kobiki, N. and Sugawara, H., “A New Concept of Compound Helicopter and Flight Tests,” Proceedings of the 2018 Asia-Pacific International Symposium on Aerospace Technology (APISAT2018), Lecture Notes in Electrical Engineering, Vol. 459, Springer, Singapore, June 2019, pp. 1343-1352.
[21] Tanabe, Y., and Saito, S., “Significance of all-Speed Scheme in Application to Rotorcraft CFD Simulations,” Proceedings of 3rd International Basic Research Conference on Rotorcraft Technology, Nanjing Univ. of Aeronautics and Astronautics Paper 23, Nanjing, China, Oct. 2009.
[22] Tanabe, Y., Saito, S., Takayama, O., Sasaki, D., and Nakahashi, K., “A New Hybrid Method of Overlapping Structured Grids Combined with Unstructured Fuselage Grids for Rotorcraft Analysis,” Proceedings of 36th European Rotorcraft Forum, Association Aeronautique et Astronautique de France Paper 071, Paris, France, Sept. 2010.
[23] Tanabe, Y., Saito, S., and Sugawara, H., “Evaluation of Rotor Noise Reduction by Active Devices Using a CFD/CSD Coupling Analysis Tool Chain,” Proceedings of 1st Asian/Australian Rotorcraft Forum, ARF 2012 Executive Committee Paper A-IV-1_P107_F, Busan, Korea, Feb. 2012.
[24] Tanabe, Y., Saito, S., and Sugawara, H., “Construction and Validation of an Analysis Tool Chain for Rotorcraft Active Noise Reduction,” Proceedings of 38th European Rotorcraft Forum, Nederlandse Vereniging voor Luchtvaarttechniek Paper ERF2012_025, Amsterdam, Netherlands, Sept. 2012.
[25] Jameson, A. and Baker, T. J., “Solution of the Euler equations for Complex Configuration,” Proceedings of 6th Computational Fluid Dynamics Conference Danvers, AIAA Paper 83-1929, Danvers, MA, USA, July 1983.
[26] Zhang, L. P., and Wang, Z. J., “A Block LU-SGS Implicit Dual Time-Stepping Algorithm for Hybrid Dynamic Meshes,” Computers & Fluids, Vol. 33, No. 7, 2004, pp. 891–916.
[27] Yamamoto, S., and Daiguji, H., “Higher-Order-Accurate Upwind Schemes for Solving the Compressible Euler and Navier-Stokes Equations,” Computers & Fluids, Vol. 22, Nos. 2–3, 1993, pp. 259–270.
[28] Menter, F. R., Kuntz, M., and Langtry, R., “Ten Years of Industrial Experience with the SST Turbulence Model,” Turbulence, Heat and Mass Transfer, Vol. 4, edited by K. Hanjalic, Y. Nagano, and M. Tummers, Begell House, Inc., 2003, pp. 625–632.
[29] Prouty, R.W., Helicopter Performance, Stability, and Control, Krieger, Malabar, FL, 2005, p. 698.
[30] Bonet, J. and Peraire, J., “An Alternating Digital Tree (ADT) Algorithm for 3D Geometric Searching and Intersection Problems,” International Journal for Numerical Methods in Engineering, Vol. 31, pp. 1-17, 1991.
[31] Hayami, K., Sugawara, H., Tanabe, Y., and Kameda, M., “Numerical Investigation of Aerodynamic Interference on Coaxial Rotor,” Proceedings of AIAA Scitech 2020 Forum, AIAA Paper AIAA 2020-0306, Orlando, FL, Jan. 2020.